VIP Defect Engineering Very Important Paper

DOI: 10.1002/anie.201410031

Half-Metallicity in Single-Layered Manganese Dioxide Nanosheets by Defect Engineering**

Hui Wang, Jiajia Zhang, Xudong Hang, Xiaodong Zhang, Junfeng Xie, Bicai Pan, and Yi Xie**

Abstract: *Defect engineering is considered as one of the most efficient strategies to regulate the electronic structure of materials and involves the manipulation of the types, concentrations, and spatial distributions of defects, resulting in unprecedented properties. It is shown that a single-layered MnO_2 nanosheet with vacancies is a robust half-metal, which was confirmed by theoretical calculations, whereas vacancy-free single-layered MnO_2 is a typical semiconductor. The half-metallicity of the single-layered MnO_2 nanosheet can be observed for a wide range of vacancy concentrations and even in the co-presence of Mn and O vacancies. This work enables the development of half-metals by defect engineering of well-established low-dimensional materials, which may be used for the design of next-generation paper-like spintronics.*

Half-metals, with a metallic nature for one spin and an insulating/semiconducting nature for the opposite spin, are considered as ideal materials for applications in spintronics, because their carriers are theoretically 100% spin-polarized.[1,2] To date, various half-metals have been reported, which are mainly based on bulk oxides, Heusler alloys, or perovskites, whereas attention has rarely been paid to the half-metallicity in low-dimensional materials.[3–6] Along with the rapid development of graphene, the interest in ultrathin two-dimensional (2D) nanosheets has been growing exponentially owing to their unique and diverse electronic structures.[7–11] Ultrathin 2D nanosheets with single- or few-layer thickness can exhibit properties that are totally different to those of their bulk counterparts, which offers further opportunities for the development of half-metallic 2D crystals.[12–15] Furthermore, ultrathin 2D nanosheets can be used as building blocks of ultrathin, transparent, and flexible electronic devices, rendering them promising and noteworthy candidates for the design of next-generation spintronics.[7]

[*] H. Wang,[+] J. J. Zhang,[+] X. Hang, Dr. X. D. Zhang, Dr. J. F. Xie, Prof. B. C. Pan, Prof. Y. Xie
Hefei National Laboratory for Physical Science at Microscale
Collaborative Innovation Center of Chemistry for Energy Materials
University of Science and Technology of China
Hefei, Anhui, 230026 (P.R. China)
E-mail: zhxid@ustc.edu.cn
yxie@ustc.edu.cn

[+] These authors contributed equally to this work.

[**] We thank the National Natural Science Foundation of China (11079004, 21331005, 11321503, 21401181), the Chinese Academy of Science (XDB01020300), the China Postdoctoral Science Foundation (BH2060140013), and the Fundamental Research Funds for the Central University (WK2060190032) for financial support.

Supporting information for this article is available on the WWW under http://dx.doi.org/10.1002/anie.201410031.

Although a few 2D nanosheets have been predicted to exhibit half-metallicity, only a few categories have been described, and these nanosheets can hardly be obtained experimentally.[14–19] Therefore, exploring effective strategies to regulate the electronic structures of well-established materials seems to be a desirable way to pursue half-metallicity in 2D nanosheets of practical value. Among the various strategies, defect engineering is one of the most effective ways to regulate the electronic properties of materials.[20–22] Through defect engineering, the electronic structures of materials can be significantly changed even with very low vacancy or dopant concentrations, which could be as low as one vacancy/dopant per one hundred million host atoms. Bearing this in mind, we herein focused on manganese dioxide (MnO_2), whose single-layered nanosheets were predicted to show intrinsic ferromagnetic properties with a high Curie temperature,[23] so that it should be possible to render the MnO_2 nanosheet half-metallic by further defect engineering. As an important semiconductor, MnO_2 has been applied in a variety of areas, including catalysis and energy storage.[24,25] Furthermore, MnO_2 can be easily exfoliated into ultrathin nanosheets owing to the layered structure of the manganese oxide precursors, and defects can be readily introduced into the as-prepared nanosheets during the synthetic processes.[25–28]

Herein, single-layered MnO_2 nanosheets with Mn vacancies were synthesized by exfoliation of their bulk counterparts in solution, as reported previously.[27,28] In detail, a defective layered manganese oxide precursor (K_xMnO_2) was first prepared by decomposition of $KMnO_4$ at high temperature. Then, the as-obtained K_xMnO_2 was exfoliated into single-layered nanosheets by proton exchange. The concentration of Mn vacancies for the as-prepared nanosheets can be easily tuned by controlling the temperature at which K_xMnO_2 is prepared in the first step, the lower the temperature, the more vacancies exist.[28]

The morphology and structure of the as-obtained product were studied in detail. As can be seen from the transmission electron microscopy (TEM) and scanning electron microscopy (SEM) images (Figure 1a,b), the as-obtained product shows sheet morphology with a size ranging from several hundred nanometers to a few micrometers. The as-prepared nanosheets can be readily assembled into large-area films of tunable thickness by a vacuum-filtration method, which can then be transferred onto different substrates for further practical applications (Supporting Information, Figure S4). The thickness of the as-prepared nanosheets was measured by atomic force microscopy (AFM; Figure 1c,d); it can be clearly seen that the thickness of the nanosheet is only approximately 0.4 nm, which corresponds to single-layer

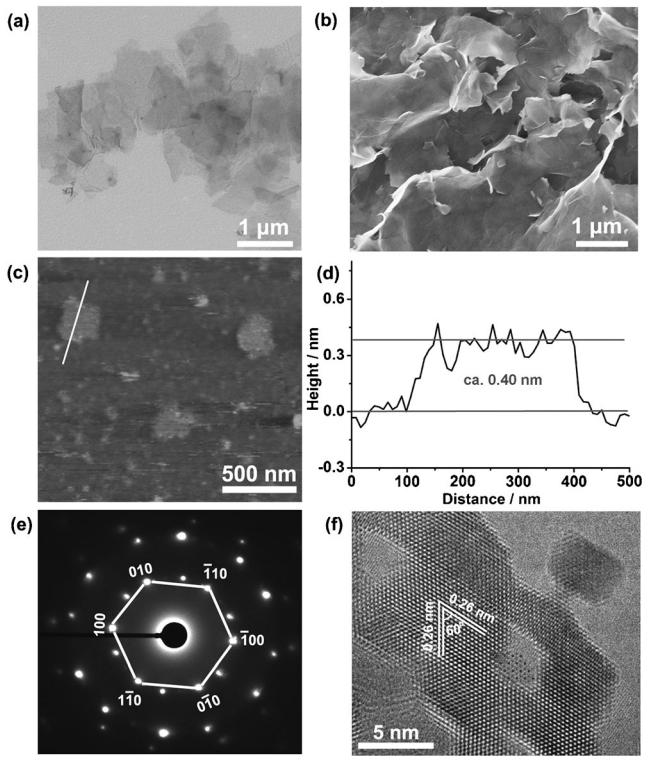

Figure 1. Morphology and structural characterization of the prepared nanosheet. a) TEM image. b) SEM image. c) AFM image. d) Corresponding height image. e) SAED pattern. f) HRTEM image.

MnO_2. The high-resolution TEM (HRTEM) image and the corresponding selected-area electron diffraction (SAED) pattern (Figure 1 e,f) reveal the single-crystal characteristics of the nanosheet. The lattice fringes of 2.6 Å correspond to the {100} lattice plane of the MnO_2 crystal. Irregular holes with sizes ranging from several angstroms (Å) to a few nanometers are also present in the single-crystalline nanosheets (Figure 1 f and Figure S3), indicating the presence of numerous vacancies in the as-obtained nanosheet. Unlike previously reported, the observation of small holes indicates that there are not only Mn vacancies, but also O vacancies in the single-layered MnO_2 nanosheets. It is anticipated that the chemical environments of Mn and O around the holes will be different to those of their hole-free counterpart, which results in unprecedented electronic properties of the as-prepared single-layered MnO_2 nanosheets. A high-angle annular dark-field scanning transmission electron microscopy (HAADF-STEM) image and the corresponding energy-dispersive spectra (EDS; Figure S1) clearly reveal the homogeneous distribution of Mn and O in the as-obtained sample with a Mn/O molar ratio estimated to be approximately 0.96:2, which is slightly below the stoichiometric ratio of MnO_2. The elemental ratio of the as-prepared samples was further studied by inductively coupled plasma atomic emission spectroscopy (ICP-AES; Table S1), which gave an average Mn/O molar ratio of approximately 0.95:2, which is in good agreement with the value estimated by EDS. Herein, we defined the amount of O as "2" and used this value to calibrate the content of Mn. Because of the co-presence of Mn and O vacancies, the formula of the as-prepared nanosheets should be written as $Mn_{1-x}\square_xO_{2-y}\triangle_y$, where $\square$ and $\triangle$ represent Mn and O vacancies, respectively. The percentage of Mn vacancies was approximately 4–5% without considering the number of O vacancies, which would be underestimated owing to the co-presence of Mn and O vacancies in the as-prepared nanosheets. Although it is difficult to determine the accurate amount of Mn and O vacancies in the as-prepared nanosheets, the concentration of Mn vacancies should not deviate too much from the 4–5% measured experimentally.

As the defect structure of the obtained single-layered MnO_2 nanosheets is unique, it is essential to study their electronic properties and potential practical applications. Herein, we carried out first-principles calculations to explore the electronic structures of the single-layered MnO_2 nanosheets with different vacancy concentrations and distributions, namely with only Mn vacancies, only O vacancies, or with both Mn and O vacancies. A slab was built to mimic the structure of single-layered MnO_2, which is composed of MnO_6 octahedra that share edges; manganese ions occupy the centers of the octahedra and are coordinated to the six nearest oxygen ions, while each oxygen ion is coordinated to three nearest manganese ions.

As shown in Figure 2 c, a Mn vacancy is introduced into the slab of single-layered MnO_2 with a Mn vacancy concentration of approximately 6.25%. The corresponding calculated density of states (DOS) of the slab above is spin-polarized at the Fermi level (Figure 2 d). In detail, the curves for the spin-down states show semiconducting behavior with a bandgap of approximately 1.65 eV, while the curves for the spin-up states are metallic. These results unequivocally indicate the half-metallic behavior of single-layered MnO_2 nanosheets with Mn vacancies. The half-metallic gap of the slab was predicted to be as large as 1.6 eV, which indicates that the single-layered MnO_2 nanosheet with Mn vacancies is an ideal candidate for spintronics. As can be clearly seen from the charge density distributions near the Fermi level (Figure 2 c), the half-metallic behavior of the MnO_2 slab with Mn vacancies is mainly due to the hybridization of neighboring O 2p and Mn 3d orbitals around the Mn vacancies, whereas the other atoms have little influence on the half-metallicity of the slab. For comparison, the DOS of a 4×4 slab of MnO_2 without vacancies was also studied (Figure 2 b), and showed a typical semiconducting character. The results above strikingly indicate the crucial role of the Mn vacancies for the half-metallic character of the single-layered MnO_2 nanosheet. However, when only O vacancies were introduced, the slab of single-layered MnO_2 remained semiconducting, indicating that only the presence of O vacancies cannot change the semiconducting nature of single-layered MnO_2 (Figure S7).

It has been well accepted that the vacancy concentration is a crucial variable when determining the electronic structure of materials. To investigate the influence of the Mn vacancy concentration on the electronic structure of single-layered MnO_2, we built 3×3, 5×5, and 6×6 slabs of MnO_2 with one Mn vacancy each, and the Mn vacancy concentrations were estimated to be 11.1%, 4%, and 2.8%, respectively. The slab models and corresponding DOS are presented in Figure S6,

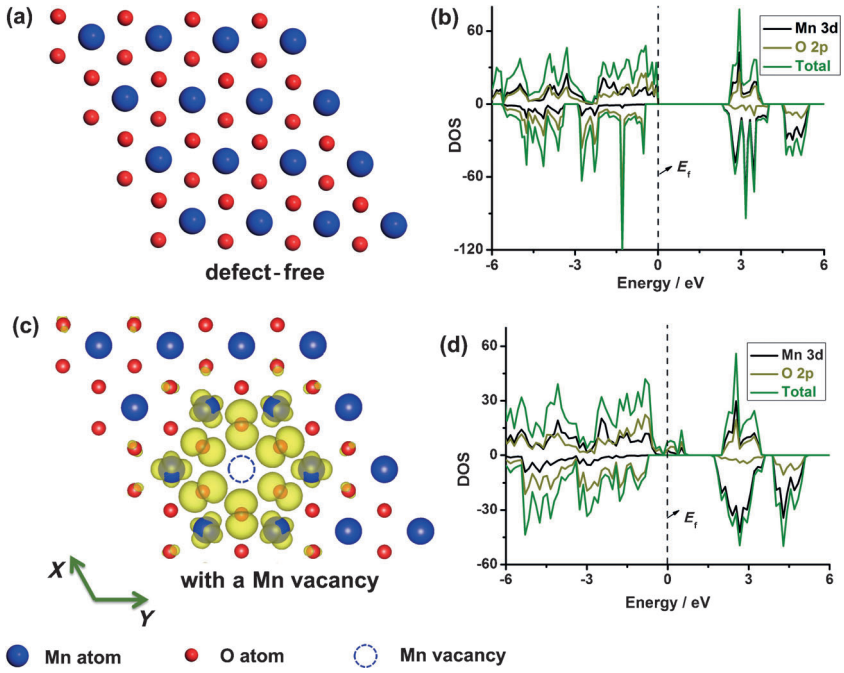

Figure 2. a) A 4×4 slab of defect-free MnO_2. b) DOS of defect-free MnO_2. c) Charge density distributions of a 4×4 slab with a Mn vacancy near the Fermi level, as represented by the isosurfaces around the Mn and O atoms. d) DOS of the MnO_2 slab with a Mn vacancy.

Table 1: Influence of the Mn vacancy concentration on the conductive nature of single-layered MnO_2 slabs. "↓" refers to the spin-down DOS of the slabs.

Slab model	Mn vacancy concentration [%]	Conductive nature	Band gap [eV]
4×4	0	semiconducting	2.28
6×6	2.8	half-metallic	1.81 (↓)
5×5	4.0	half-metallic	1.78 (↓)
4×4	6.25	half-metallic	1.65 (↓)
3×3	11.1	half-metallic	1.23 (↓)

and the results are summarized in the Table 1. As can be seen from Figure S6, an increase or decrease in the Mn vacancy concentration does not change the half-metallic nature of single-layered MnO_2. It is interesting that the half-metallic gaps in the spin-down states decrease from 1.81 eV to 1.23 eV with an increase in the Mn vacancy concentration from 2.8% to 11.1%. It is well accepted that a large half-metallic gap can enhance the stability of half-metallicity in materials by preventing possible spin flip transitions. In this case, one may wonder whether the increase in the Mn vacancy concentration would induce the instability of half-metallicity in single-layered MnO_2? In fact, the half-metallic gap of the MnO_2 nanosheet with a Mn vacancy concentration of 11.1% is so large (ca. 1.23 eV) that its possible spin flip transitions are prevented at ambient temperature, indicating that the half-metallicity of single-layered MnO_2 nanosheet can be observed for a wide range of Mn vacancy concentrations.

Once cation vacancies have been introduced into a crystal structure, it is unavoidable that anion vacancies emerge simultaneously. In this study, Mn and O vacancies are both present in the single-layered MnO_2 nanosheet, as illustrated experimentally. It is thus essential to investigate the electronic structure of single-layered MnO_2 in the presence of both Mn and O vacancies. 4×4 slabs with one Mn and one O vacancy at different distances were considered. The models with the longest and shortest distances between the Mn and O vacancies are presented in Figure 3a and Figure 3c, respectively, and the other two models are displayed in Figure S8. As can be seen from the corresponding DOS, all of the slabs show robust half-metallic character, indicating that the half-metallicity of single-layered MnO_2 nanosheets can be maintained even in the co-presence of Mn and O vacancies. However, unlike for the slab with only Mn vacancies, atoms around the O vacancies also contribute to the half-metallicity of the slabs in the co-presence of Mn and O vacancies, as confirmed by the corresponding charge density distributions (Figure 3a,c). Furthermore, the O vacancies also have a strong influence on the charge density distributions of the elements around the Mn vacancies, and the shorter the distance between the O and Mn vacancies is, the stronger the influence will be.

To visualize the spin distribution for single-layered MnO_2 in the co-presence of Mn and O vacancies and for its defect-free counterpart, the corresponding spin densities are plotted in Figure 4. Clearly, the magnetic moment distribution in single-layered MnO_2 is mainly influenced by the Mn atoms with a magnetic moment of approximately 3 μB on each Mn site. The O atoms around the Mn vacancies also contribute to the magnetic moments of the defective single-layered MnO_2 with a magnetic moment of about −0.25 μB on each O site. The directions of the magnetic moments for Mn and O differ from each other. Because of the small magnetic moment of O, the magnetic moment distributions of single-layered MnO_2 with or without vacancies are similar.

Although the concept of half-metallicity has been generally accepted, there is still a lack of simple and effective experiments to prove or disprove the half-metallicity.[29,30] Electronic structure calculations still play one of the most important roles in identifying and searching for new half-metallic materials.[31] In this study, all of the theoretical calculations indicate that the half-metallicity in a single-layered MnO_2 nanosheet can be successfully achieved by defect engineering, and that single-layered MnO_2 nanosheets with vacancies may be a new half-metal. Although a few studies have predicted that half-metallicity can be derived from vacancies, the vacancies must stay at specific lattice sites with a fixed concentration, which has undoubtedly hindered their experimental exploitation.[32–34] Unlike in previous reports, the half-metallicity of single-layered MnO_2 nanosheets can be observed for a wide range of vacancy concentration and even in the co-presence of Mn and O vacancies. In

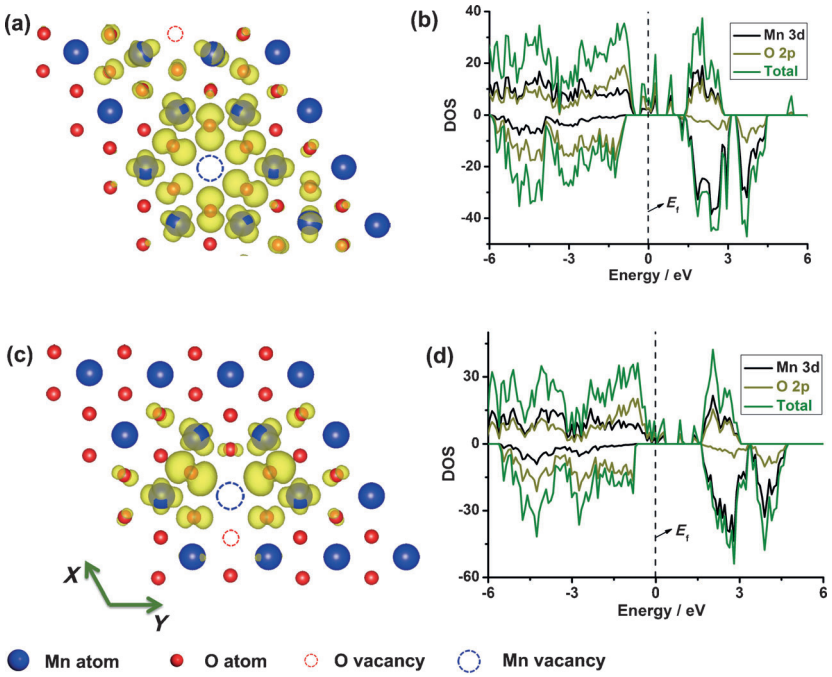

Figure 3. a, c) Charge density distributions of a 4×4 slabs with both a Mn and an O vacancy at different distances, as represented by the isosurfaces around the Mn and O atoms. b, d) Corresponding DOS of the slabs presented in (a) and (c), respectively.

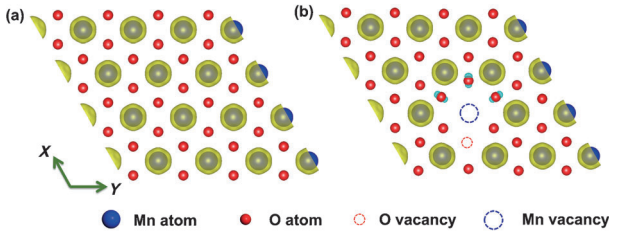

Figure 4. a, b) Calculated spin densities ($\rho\uparrow-\rho\downarrow$) of a 4×4 slab of defect-free MnO_2 (a) and MnO_2 with both a Mn and an O vacancy (b). The isosurfaces around the Mn and O atoms represent their spin density distributions.

that case, the possibilities for experimentally introducing half-metallicity into MnO_2 nanosheets by defect engineering are greatly increased. Single-layered MnO_2 nanosheets with vacancies would be the first artificial 2D crystals with robust half-metallicity that can be observed for a wide range of vacancy concentrations.

In summary, we have shown that a single-layered MnO_2 nanosheet with vacancies is a new half-metallic 2D crystal, as confirmed by calculations. The as-prepared nanosheets feature small holes with sizes ranging from several angstroms to a few nanometers, giving direct evidence for the presence of numerous vacancies (both Mn and O vacancies) in single-layered MnO_2 nanosheets. The half-metallicity of the single-layered MnO_2 nanosheets can be observed for a wide range of vacancy concentrations and even in the co-presence of Mn and O vacancies. Furthermore, owing to the ultrathin nature of the as-prepared MnO_2 nanosheet, it can be assembled into a transparent and flexible film for the design of next-generation spintronics. The half-metallicity of single-layered MnO_2 with vacancies will not only inspire the design of new half-metals by defect engineering of well-established low-dimensional materials, but also pave the way for the design of new spintronics.

Experimental Section

All calculations were performed using the VASP code,[35] with the projector augmented wave approach,[36] and utilizing the screened hybrid functional as proposed by Heyd, Scuseria, and Ernzerhof (HES).[37] The value of exact nonlocal exchange (a) was chosen to be 10%, which yielded a band gap of 2.28 eV, which is in excellent agreement with the experimentally measured band gap of 2.23 eV.[24] We applied periodic boundary conditions with a vacuum space of 15 Å to avoid interactions between two sheets in nearest-neighbor unit cells. We set the energy cutoff and the convergence criteria for energy and force to be 400 eV, 10^{-4} eV, and 0.02 eV Å^{-1}, respectively. The k point grids for the 6×6, 5×5, 4×4, and 3×3 slabs of MnO_2 were chosen to be 1×1×1, 2×2×1, 4×4×1, and 5×5×1, respectively.

Received: October 13, 2014
Published online: November 25, 2014

Keywords: defect engineering · half-metallicity · manganese dioxide · nanosheets

[1] S. A. Wolf, D. D. Awschalom, R. A. Buhrman, J. M. Daughton, S. von Molnár, M. L. Roukes, A. Y. Chtchelkanova, D. M. Treger, *Science* **2001**, *294*, 1488.
[2] R. A. de Groot, F. M. Mueller, P. G. V. Engen, K. H. J. Buschow, *Phys. Rev. Lett.* **1983**, *50*, 2024.
[3] X. Li, X. Wu, J. Yang, *J. Am. Chem. Soc.* **2014**, *136*, 5664.
[4] V. Alijani, J. Winterlik, G. H. Fecher, S. S. Naghavi, C. Felser, *Phys. Rev. B* **2011**, *83*, 184428.
[5] N. Kobayashi, K. Nishida, *Nature* **1998**, *395*, 357.
[6] S. K. Kwon, S. J. Youn, B. I. Min, *Phys. Rev. B* **2000**, *62*, 357.
[7] X. Zhang, Y. Xie, *Chem. Soc. Rev.* **2013**, *42*, 8187.
[8] X. Huang, Z. Zeng, H. Zhang, *Chem. Soc. Rev.* **2013**, *42*, 1934.
[9] X. Huang, C. Tan, Z. Yin, H. Zhang, *Adv. Mater.* **2014**, *26*, 2185.
[10] X. Zhang, J. Xu, H. Wang, J. Zhang, H. Yan, B. Pan, J. Zhou, Y. Xie, *Angew. Chem. Int. Ed.* **2013**, *52*, 4361; *Angew. Chem.* **2013**, *125*, 4457.
[11] X. Zhang, X. Xie, H. Wang, J. Zhang, B. Pan, Y. Xie, *J. Am. Chem. Soc.* **2013**, *135*, 18.
[12] K. Xu, P. Chen, X. Li, C. Wu, Y. Guo, J. Zhao, X. Wu, Y. Xie, *Angew. Chem. Int. Ed.* **2013**, *52*, 10477; *Angew. Chem.* **2013**, *125*, 10671.
[13] H. Li, J. Wu, Z. Yin, H. Zhang, *Acc. Chem. Res.* **2014**, *47*, 1067.
[14] X. Zhang, J. Zhang, J. Zhao, B. Pan, M. Kong, J. Chen, Y. Xie, *J. Am. Chem. Soc.* **2012**, *134*, 11908.
[15] X. Li, X. Wu, J. Yang, *J. Am. Chem. Soc.* **2014**, *136*, 11065.
[16] E. Kan, W. Hu, C. Xiao, R. Lu, K. Deng, J. Yang, H. Su, *J. Am. Chem. Soc.* **2012**, *134*, 5718.
[17] E. J. Kan, H. J. Xiang, F. Wu, C. Tian, C. Lee, J. L. Yang, M.-H. Whangbo, *Appl. Phys. Lett.* **2010**, *97*, 122503.

[18] Y.-W. Son, M. L. Cohen, S. G. Louie, *Nature* **2006**, *444*, 347.
[19] A. Hashmi, J. Hong, *Sci. Rep.* **2014**, *4*, 4374.
[20] J. Lahiri, Y. Lin, P. Bozkurt, I. I. Oleynik, M. Batzill, *Nat. Nanotechnol.* **2010**, *5*, 326.
[21] J. B. Yi, C. C. Lim, G. Z. Xing, H. M. Fan, L. H. Van, S. L. Huang, K. S. Yang, X. L. Huang, X. B. Qin, B. Y. Wang, T. Wu, L. Wang, H. T. Zhang, X. Y. Gao, T. Liu, A. T. S. Wee, Y. P. Feng, J. Ding, *Phys. Rev. Lett.* **2010**, *104*, 137201.
[22] K. D. Kwon, K. Refson, G. Sposito, *Phys. Rev. Lett.* **2008**, *100*, 146601.
[23] M. Kan, J. Zhou, Q. Sun, Y. Kawazoe, P. Jena, *J. Phys. Chem. Lett.* **2013**, *4*, 3382.
[24] N. Sakai, Y. Ebina, K. Takada, T. Sasaki, *J. Phys. Chem. B* **2005**, *109*, 9651.
[25] Y. Omomo, T. Sasaki, L. Wang, M. Watanabe, *J. Am. Chem. Soc.* **2003**, *125*, 3568.
[26] P. Ruetschi, R. Giovanoli, *J. Electrochem. Soc.* **1988**, *135*, 2663.
[27] L. Wang, Y. Omomo, N. Sakai, K. Fukuda, I. Nakai, Y. Ebina, K. Takada, M. Watanabe, T. Sasaki, *Chem. Mater.* **2003**, *15*, 2873.
[28] A.-C. Gaillot, V. A. Drits, A. Manceau, B. Lanson, *Microporous Mesoporous Mater.* **2007**, *98*, 267.
[29] K. E. H. M. Hanssen, P. E. Mijnarends, L. P. L. M. Rabou, K. H. J. Buschow, *Phys. Rev. B* **1990**, *42*, 1533.
[30] J.-H. Park, E. Vescovo, H.-J. Kim, C. Kwon, R. Ramesh, T. Venkatesan, *Nature* **1998**, *392*, 794.
[31] M. I. Katsnelson, V. Y. Irkhin, L. Chioncel, A. I. Lichtenstein, R. A. de Groot, *Rev. Mod. Phys.* **2008**, *80*, 315.
[32] Z. Zhu, Y. Cheng, U. Schwingenschlögl, *Phys. Rev. B* **2011**, *84*, 113201.
[33] Y. Chen, W. Mi, G. Chen, Q. Song, S. Guo, *Comput. Mater. Sci.* **2014**, *81*, 212.
[34] S. Picozzi, C. Ma, Z. Yang, R. Bertacco, M. Cantoni, A. Cattoni, D. Petti, S. Brivio, F. Ciccacci, *Phys. Rev. B* **2007**, *75*, 094418.
[35] G. Kresse, J. Furthmüller, *Phys. Rev. B* **1996**, *54*, 11169.
[36] G. Kresse, D. Joubert, *Phys. Rev. B* **1999**, *59*, 1758.
[37] S. Heyd, G. E. Scuseria, M. Ernzerhof, *J. Chem. Phys.* **2003**, *118*, 8207.

